

A Modified Spin Pulsed Readout Method for NV Center Ensembles Reducing Optical Noise

Jixing Zhang¹, Heng Yuan¹, Ning Zhang¹, Lixia Xu¹, Guodong Bian¹, Pengcheng Fan¹,
Mingxin Li¹, Zhi Zhan¹, and Kan Yu²

Abstract—The optical-noise-limited spin readout sensitivity determines the precision of quantum measurement based on nitrogen-vacancy (NV) center. This article investigates the fluorescence dynamics of NV centers by solving the optical rate equations and obtains complete theoretical formulas for the existing optical spin readout method. A transfer coefficient of optical noise to signal noise in the existing differential methods at different frequencies is introduced so as to analyze the optical noise suppression ability and the signal-to-noise ratio (SNR) results under the influence of photon shot noise and optical noise. To further reduce the influence of optical noise on the signal, we propose a modified method to minimize the transfer coefficient by adding a first-order compensation term. Compared with conventional methods, our modified method showed a twofold optical noise suppression ability improvement in the measurement frequency bandwidth. The experiment proves that the final SNR is increased by 43.4% for a long-term measurement. This modified method should lead to immediate improvements in pulsed spin readout of NV center ensembles without extra instrumentation for applications in magnetic field, electric field, and temperature measurements.

Index Terms—Nitrogen-vacancy (NV) center ensemble, pulsed spin readout, rate equations.

I. INTRODUCTION

THE quantum measurements based on the negatively charged nitrogen-vacancy (NV) center in diamond have been a hot topic in the past decade according to their large

Manuscript received June 3, 2019; revised September 17, 2019; accepted October 7, 2019. Date of publication October 29, 2019; date of current version June 9, 2020. This work was supported by the National Key R&D Program of China (2016YFB0501600); the Projects of National Natural Science Foundation of China under Grant No. 61773046, 61773046, 61721091, 11575062, and 11665004; the Projects of Beijing Academy of Quantum Information Sciences under Grant No. Y18G33. The Associate Editor coordinating the review process was Yasutaka Amagai. (Corresponding authors: Heng Yuan; Ning Zhang.)

J. Zhang, L. Xu, G. Bian, P. Fan, M. Li, and Z. Zhan are with the School of Instrumentation and Optoelectronic Engineering, Beihang University, Beijing 100191, China.

H. Yuan is with the School of Instrumentation and Optoelectronic Engineering, Beihang University, Beijing 100191, China, also with the Research Institute of Frontier Science, Beihang University, Beijing 100191, China, also with the Beijing Advanced Innovation Center for Big Data-Based Precision Medicine, Beihang University, Beijing 100191, China, and also with the Beijing Academy of Quantum Information Sciences, Beijing 100193, China (e-mail: hengyuan@buaa.edu.cn).

N. Zhang is with the Zhejiang Lab, Quantum Sensing Center, Hangzhou 310000, China (e-mail: ningzhang@zhejiang.com).

K. Yu is with the School of Engineering and Mathematical Sciences, La Trobe University, Melbourne, VIC 3552, Australia.

Color versions of one or more of the figures in this article are available online at <http://ieeexplore.ieee.org>.

Digital Object Identifier 10.1109/TIM.2019.2949321

dynamics range and excellent stabilities compared with conventional quantum sensors like spin-exchange relaxation-free atomic magnetometer [1], [2]. There are many measurement applications that use the electron spin of NV center, including magnetic field measurements [3], [4], temperature measurements [5], [6], nuclear magnetic resonance [7], [8], and neuroscience [9]. These applications rely on efficient readout of the spin projection and mostly use pulsed schemes. Because the photoluminescence is affected by the spin projection in NV centers, fluorescence signals can be used for spin readout [10], [11]. To achieve higher sensitivity, a variety of experimental techniques have been proposed to improve the light collection efficiency [12], [13], [25], microwave manipulation methods [14], [15], and signal extraction using a lock-in amplifier [5], [9]. Spin readout schemes based on different principles have also been proposed, such as low-temperature resonant excitation readout [16], electric spin readout [17], and singlet infrared absorption [18]. In addition, various post-processing methods for spin readout have been proposed, including photon averaging, threshold detection [19] and maximum likelihood estimation [20], nuclear-assisted readout [21], [22], maximal adaptive-decision [23], and machine learning [24].

Although the above methods can effectively improve the efficiency of spin readout, there is still an experimental challenge in the spin projection pulse detection scheme for the NV center ensemble, which is mainly used in high-precision quantum measurement. The challenge is that the actual NV center spin readout system's optical power noise is much larger than the quantum projection noise and photon shot noise in a low-frequency scenario. This drawback leads to a fact that the actual spin readout sensitivity based on the NV ensemble is far worse than the sensitivity of single NV center divided by the square root of the number of participated NV centers in the same experimental setup. To overcome this defect, the differential detection (DD) methods are applied [4], [26], [27]. One of these approaches involves splitting the excitation laser pulse and using one laser beam as the reference signal and a balanced detector to get the differential signal. This method increases the complexity of the light path, which is a drawback. Another approach involves the use of additional pulsed fluorescent signals as the reference signal [26]–[28], [38]. Unlike the previous method, this method can eliminate the instability of laser without additional complexity.

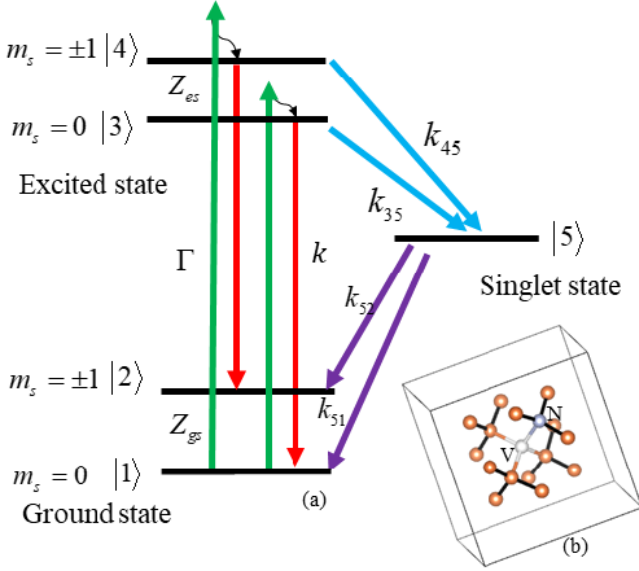


Fig. 1. (a) Energy structure of NV center. (b) Structure of NV center in diamond crystal.

In this report, to further suppress the optical noise, we established an optical dynamic mathematical model based on the rate equations and obtained the solution of this model. With this solution, the inhibition of noise at different frequencies and the optimal measurement condition were determined. Moreover, the limitations of the existing DD methods were addressed in this article. Finally, we proposed an improved DD method and conducted the spin readout sensitivity experiment and Allen deviation experiment for verifications of the modified method. This improved method further pushes the sensitivity of the quantum measurement system based on NV center ensemble to the verge of the shot noise limitation.

II. MATHEMATICAL SOLUTION

A. Optical Dynamic Model Establishment

The six-electron model of the negative NV center has been well-established in the past decades by theoretical researches [29]–[31] and experimental researches [32], [33], and there are two unpaired electrons in the e molecular orbitals (MOs) of the C_{3v} point group. As shown in Fig. 1(b), the $N - V$ axis is the C_{3v} axis. The optical transition loop for initialization is shown in Fig. 1(a). The ground states of the NV center are spin triplet with a 2.87-GHz zero field splitting value between $|1\rangle$ ($m_s = 0$) and $|2\rangle$ ($m_s = \pm 1$). The electrons in the ground states can be optically pumped into the excited state by a photon with energy larger than 1.945 eV through spin-conserving processing. The excited states also have a zero field split ($Z_{es} = 1.4$ GHz) between two substates $|3\rangle$ and $|4\rangle$. Decays of the excited states are possible through two paths: 1) spin-independent radiative decay to the same m_s ground state and emission of a 637-nm photon with rate $k_{31} = k_{42} = k$ and 2) non-radiative decay to the singlet state $|5\rangle$ with spin-dependent rates k_{45} and k_{35} [32]. Here, each k_{ij} denotes the transition rate for state $|i\rangle$ to state $|j\rangle$. The decay

from singlet $|5\rangle$ to the ground states is also spin-dependent with two decay rates k_{51} and k_{52} . These two spin-dependent decays are responsible for spin optical polarization of NV center. All relaxation rate parameters are selected from [33]. The optical pumping rate $\Gamma = k_{31} = k_{42}$ from the ground states to the excited states is proportional to excitation light power.

According to this model, we use the optical rate equations [34], [35] to build a mathematical model as follows:

$$\begin{aligned} \frac{d\rho_1}{dt} &= k \cdot \rho_3 + k_{51} \cdot \rho_5 - \Gamma \cdot \rho_1 \\ \frac{d\rho_2}{dt} &= k \cdot \rho_4 + k_{52} \cdot \rho_5 - \Gamma \cdot \rho_2 \\ \frac{d\rho_3}{dt} &= \Gamma \cdot \rho_1 - k \cdot \rho_3 - k_{35} \cdot \rho_3 \\ \frac{d\rho_4}{dt} &= \Gamma \cdot \rho_2 - k \cdot \rho_4 - k_{45} \cdot \rho_4 \\ \frac{d\rho_5}{dt} &= k_{35} \cdot \rho_3 + k_{45} \cdot \rho_4 - k_{51} \cdot \rho_5 - k_{52} \cdot \rho_5. \end{aligned} \quad (1)$$

Here, ρ_i is denoted as the i th state's population, and thus, $\sum \rho_i = 1$. It can be rewritten as a matrix form by defining $\vec{\rho} = (\rho_1, \rho_2, \rho_3, \rho_4, \rho_5)$

$$\vec{\rho}' = A\vec{\rho} \quad (2)$$

where

$$A = \begin{bmatrix} -\Gamma & 0 & k & 0 & k_{51} \\ 0 & -\Gamma & 0 & k & k_{52} \\ \Gamma & 0 & -k - k_{35} & 0 & 0 \\ 0 & \Gamma & 0 & -k - k_{45} & 0 \\ 0 & 0 & k_{35} & k_{45} & -k_{51} - k_{52} \end{bmatrix}. \quad (3)$$

After solving this equation, A has five different eigenvalues which are denoted as E_1, E_2, E_3, E_4 , and E_5 and five linearly independent eigenvectors denoted as U_1, U_2, U_3, U_4 , and U_5 , respectively. For pulse detection scheme, the population of the excited state and the singlet state at the initial state is 0. Thus, the initial is determined by spin projection in the ground state, defined as polarizability, $P = \rho_1 / (\rho_1 + \rho_2)$. Thus, the vector form of the initial state is $\vec{\rho}(0) = (P, 1-P, 0, 0, 0)^T$. The solution of the ordinary differential equations (ODE) theory is

$$\vec{\rho}(t) = e^{At} \vec{\rho}(0) \quad (4)$$

where

$$e^{At} = [e^{E_1 t} U_1 \quad \dots \quad e^{E_5 t} U_5] [U_1 \quad \dots \quad U_5]^{-1}. \quad (5)$$

Thus, the solution is of the form $\rho_j(t) = \sum_{i=1}^5 C_j^i e^{E_i t}$, where C_j^i is a coefficient solved by (5) and is determined by both the initial value $\rho(0)$ and Γ . In addition, C_j^i and P satisfy a linear relationship at any given time. The fluorescence, which is proportional to the excited states' population $\rho_3(t) + \rho_4(t)$, is also linear with P . The solution process of (5) is as follows:

Setting

$$U_i = (u_i^1, u_i^2, u_i^3, u_i^4, u_i^5)^T \quad (6)$$

and

$$W = [U_1 \ \dots \ U_5]^{-1} = \begin{bmatrix} w_1^1 & w_2^1 & w_3^1 & w_4^1 & w_5^1 \\ w_1^2 & w_2^2 & w_3^2 & w_4^2 & w_5^2 \\ w_1^3 & w_2^3 & w_3^3 & w_4^3 & w_5^3 \\ w_1^4 & w_2^4 & w_3^4 & w_4^4 & w_5^4 \\ w_1^5 & w_2^5 & w_3^5 & w_4^5 & w_5^5 \end{bmatrix}. \quad (7)$$

Thus

$$e^{At} = \begin{bmatrix} \sum_{i=1}^{i=5} e^{E_i t} u_i^1 w_i^1 & \dots & \sum_{i=1}^{i=5} e^{E_i t} u_i^1 w_i^5 \\ \vdots & \ddots & \vdots \\ \sum_{i=1}^{i=5} e^{E_i t} u_i^5 w_i^1 & \dots & \sum_{i=1}^{i=5} e^{E_i t} u_i^5 w_i^5 \end{bmatrix}. \quad (8)$$

Using (8), the solution of (4) is

$$\rho(t) = \begin{bmatrix} P \sum_{i=1}^{i=5} e^{E_i t} u_i^1 w_i^1 + (1-P) \sum_{i=1}^{i=5} e^{E_i t} u_i^1 w_i^2 \\ P \sum_{i=1}^{i=5} e^{E_i t} u_i^2 w_i^1 + (1-P) \sum_{i=1}^{i=5} e^{E_i t} u_i^2 w_i^2 \\ P \sum_{i=1}^{i=5} e^{E_i t} u_i^3 w_i^1 + (1-P) \sum_{i=1}^{i=5} e^{E_i t} u_i^3 w_i^2 \\ P \sum_{i=1}^{i=5} e^{E_i t} u_i^4 w_i^1 + (1-P) \sum_{i=1}^{i=5} e^{E_i t} u_i^4 w_i^2 \\ P \sum_{i=1}^{i=5} e^{E_i t} u_i^5 w_i^1 + (1-P) \sum_{i=1}^{i=5} e^{E_i t} u_i^5 w_i^2 \end{bmatrix}. \quad (9)$$

Because the fluorescence is approximately proportional to $\rho_3 + \rho_4$, the resulting function for the fluorescence is

$$f(P, t) \approx \rho_3 + \rho_4 = P \sum_{i=1}^{i=5} e^{E_i t} (u_i^3 + u_i^4) (w_1^i - w_2^i) + \sum_{i=1}^{i=5} e^{E_i t} (u_i^3 + u_i^4) w_2^i. \quad (10)$$

It should be noted that (10) implies the pumping rate Γ in u and w is related to pumping rate Γ . For the sake of simplicity, (10) is transformed into the following form:

$$\rho_{3+4}(t) = \sum_{i=1}^5 C_i e^{-E_i t} = \left(\sum_{i=1}^5 d_i(\Gamma) e^{-E_i t} \right) (P + g_i(\Gamma)) \quad (11)$$

where $g_i(\Gamma) = w_2^i / (w_1^i - w_2^i)$ and $d_i(\Gamma) = (u_i^3 + u_i^4) (w_1^i - w_2^i) w_2^i$ are the functions of pumping rate Γ . As the variables' separation for fluorescence is achieved, the integral of fluorescence S is also linear to P , given by

$$S = \int_0^{t_0} \rho_j dt = \left(\sum_{i=1}^5 d_i(\Gamma) \frac{1}{E_i} (1 - e^{-E_i t_0}) \right) (P + g_i(\Gamma)) \quad (12)$$

where t_0 is the integration time. From (12), it is evident that the integration time, pumping rate, and polarizability determine the integral S .

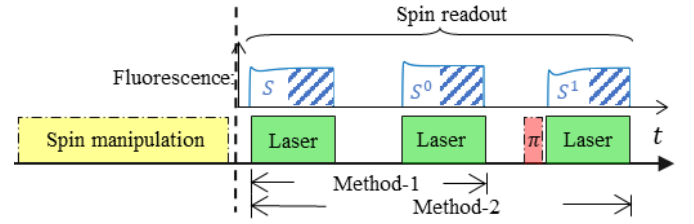


Fig. 2. Conventional pulsed spin readout sequence. The light blue line indicates the fluorescence waveform under the pulse. Sensing based on the NV color center can be divided into two steps. The first step is the initialization and manipulation of the spin, represented as the first light yellow pulse in the figure, in which there are spin sensing environmental information such as the magnetic field. The second step is the spin readout, represented as the following several pulses, which is to be studied in this article. The fluorescence integral obtained by the first laser pulse is denoted as S , corresponding to the measured polarizability P after the current spin manipulation. The fluorescence integral obtained by the second laser pulse measurement is denoted as S^0 , corresponding to the maximum polarizability P^0 at which the spin state is at $m_s = 0$ after being repumped by the first pulse. There is also a microwave pulse before the third laser pulse, which is used to generate a Rabi oscillation π pulse to flip the spin from the $m_s = 0$ state to the $m_s = 1$ state and obtain the minimum polarizability P^1 .

B. Models of Conventional DD Methods

Because the integral of fluorescence and polarizability is linear, the polarizability can be obtained through fluorescence measurements. In addition, the incident light intensity has a significant effect on the fluorescence integral. Therefore, to ensure the accuracy of the polarizability measurement, it is necessary to eliminate the influence of optical power noise. The DD method introduced earlier is described in detail here based on two sequences. As shown in Fig. 2, the first method uses the first detection pulse to detect the fluorescence integral corresponding to the current polarizability [23], [24]. A new pulse is added after the first detection pulse, and the system is repolarized to the maximum polarizability P^0 due to the influence of the first detection pulse. Therefore, the second detection pulse detects the integral of the fluorescence corresponding to P^0 and acts as a reference. Assuming that the interval between the two pulses is much smaller than the characteristic time of the optical power fluctuation, the optical power can be assumed to be constant during this detection time. Therefore, the effect of optical power noise can be eliminated by determining the difference between the two pulses. The specific algorithm has two mathematical processing methods: Method-1a involving $(S - S^0)/S^0$ and Method-1b using $S - S^0$.

For Method-1a

$$\frac{S - S^0}{S^0} = \frac{\left(\sum d_i \frac{1}{E_i} (1 - e^{-E_i t}) \right) (P - P^0)}{\left(\sum d_i \frac{1}{E_i} (1 - e^{-E_i t}) \right) (P^0 + g(\Gamma))}. \quad (13)$$

For Method-1b

$$S - S^0 = \left(\sum d_i \frac{1}{E_i} (1 - e^{-E_i t}) \right) (P - P^0). \quad (14)$$

For Method-2, as shown in Fig. 2, a microwave pulse and a detection pulse are added based on Method-1 [8]. The microwave pulse is then used to invert the spin to the case where the polarizability achieves the smallest P^1 . It is to

be noted that P^1 is greater than $I-P^0$ because the flipping efficiency cannot reach 100%. Using the integral of the fluorescence of these three pulses, we can obtain the polarizability by the following expression:

$$\frac{S - S^1}{S^0 - S^1} = \frac{(P - P^1)}{(P^0 - P^1)}. \quad (15)$$

From this result, it is evident that Methods-1a and -1b cannot suppress the optical power noise completely in principle because (13) and (14) contain the pumping-rate-related terms d_i and $g(\Gamma)$. In contrast, Method-2 can suppress this noise. There are still some limitations of this theoretical calculation, which assumes that the change in laser power is much slower than the pulse. However, the actual situation of optical noise does not necessarily meet this condition, so further investigation based on the actual situation is needed.

III. SIGNAL-TO-NOISE RATIO (SNR) ANALYSIS

It should be noted that although we aim to suppress the noise caused by laser power fluctuations, according to the basic principle of its fluorescence spin readout, the signal itself contains photon shot noise. Therefore, we first theoretically calculate the SNR of a single measurement under photon shot noise and then add the optical power noise to obtain the actual SNR. According to the principle of fluorescence collection, the noise attached to the signal itself is photon shot noise and satisfies the Poisson distribution [11]. Therefore, the variance of S is

$$\text{Var}(S) = S. \quad (16)$$

Use the definition of SNR in [11]

$$\text{SNR} = \frac{|\text{Signal}_{\max} - \text{Signal}_{\min}|}{\sqrt{\text{Var}_{\max} + \text{Var}_{\min}}}. \quad (17)$$

For a single-pulse photon summation method

$$\text{SNR}_{\text{ps}} = \frac{S^0 - S^1}{\sqrt{S^0 + S^1}}. \quad (18)$$

It can be deduced that the SNR of Method-1a is ($S^0 \approx S^1$)

$$\text{SNR}_{1a} = \frac{S^0 - S^1}{\sqrt{\frac{4(S^0)^2 - S^0 S^1 + (S^1)^2}{S^0}}} \approx \frac{\text{SNR}_{\text{ps}}}{\sqrt{2}}. \quad (19)$$

The SNR of Method-1b is

$$\text{SNR}_{1b} = \frac{S^0 - S^1}{\sqrt{2S^0 + 2S^1}} = \frac{\text{SNR}_{\text{ps}}}{\sqrt{2}}. \quad (20)$$

The SNR of Method-2 is

$$\text{SNR} = \frac{S^0 - S^1}{\sqrt{2S^1 + 4S^0}} \approx \frac{\text{SNR}_{\text{ps}}}{\sqrt{3}}. \quad (21)$$

To get the above SNR formula, we use the Taylor expansion first-order approximation of variance of reciprocal

$$\text{var}\left(\frac{1}{S}\right) \approx \frac{1}{E(S)^4} \text{Var}(S). \quad (22)$$

This approximation is established at $E(S) \gg 1$ and the condition can be well-satisfied. When the condition is not

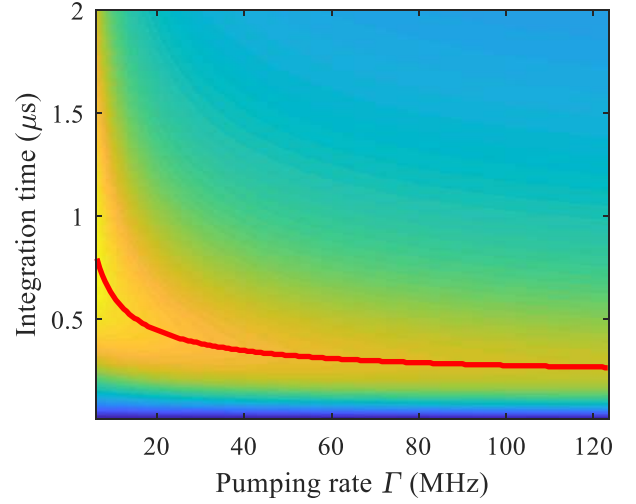


Fig. 3. Relationship between the simulated SNR results and the integration time and pumping rate.

well-satisfied, as in the case of single NV center, the variance calculated above will increase, so the difference method is more suitable for the case of the ensemble. With the theoretical formula of SNR, we can calculate the optimal single measurement SNR conditions of the existing methods, including light intensity conditions and integration time conditions. In this way, we can calculate the SNR under different conditions using the optical rate equation model and the SNR formula calculated above. The calculation results are shown in Fig. 3. The red line represents the optimal integration time at each pumping rate. The optimal integration time obtained is about 250–300 ns depending on the optical pumping rate, which is consistent with the conventional research results [11].

Next, we establish the expression of optical noise. Due to the linear relationship between the pumping rate Γ and the laser power, the change in light intensity can be expressed as Γ . Set the initial pumping rate as Γ_0 , and Γ can be expressed as $\Gamma = \Gamma_0 + \Delta\Gamma(t)$. Then the variance of the period over time can be represented by the mean square error measured by the experiment

$$\text{Var}(\Gamma) = \sum (\Delta\Gamma(t))^2. \quad (23)$$

To reflect the level of laser noise, we performed spectral analysis. The results are shown in part V. Combined with the definition of optical noise in (23), the total noise can be obtained

$$\text{Var} = \sqrt{\delta\text{Signal}(\Gamma)^2 + \text{Var}(S)} = \sqrt{\mu^2 \text{Var}(\Gamma) + \text{Var}_{\text{Signal}}} \quad (24)$$

where $\mu = \partial\text{Signal}/\partial\Gamma$ is defined as the transfer coefficient of laser power variance to signal noise caused by $\text{Var}(\Gamma)$. In this way, we can also obtain the actual SNR under both laser noise and photon shot noise, such as the actual SNR of photon summation

$$\text{SNR}_{\text{ps}} = \frac{S^0 - S^1}{\sqrt{S^0 + S^1 + 2\mu^2 \text{Var}(\Gamma)}}. \quad (25)$$

For optical noise, μ determines the transmission of laser noise to the final signal noise, so μ also represents the laser

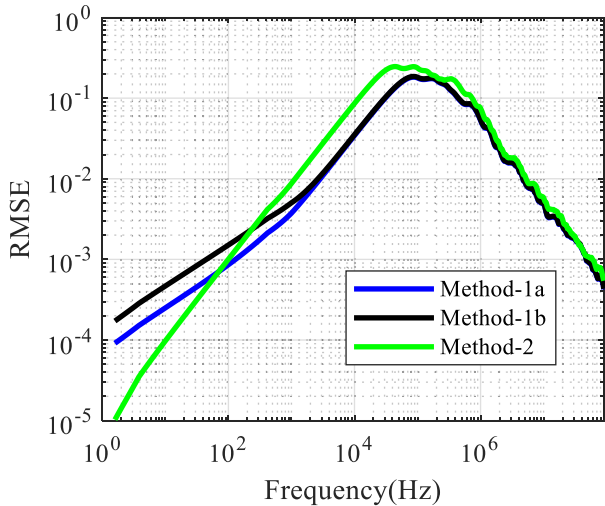


Fig. 4. Simulation results of the noise suppression capability of different frequency bands by different differential methods. The blue curve and black curve represent Methods-1a and 1b's normalized noise amplitude, respectively. They exhibit a significant increase in the low-frequency band. The green curve represents Method-2's normalized noise amplitude.

noise suppression capability of different differential methods. Because the change in light intensity satisfies (23), we use simulation to analyze the magnitude of μ for noise at different frequencies. The simulation model discretizes the dynamic equation with a time interval $\Delta t = 1\text{ns}$, expressed as

$$\rho_i(t_k) = \left(\sum_j k_{ji} \cdot \rho_j(t_{k-1}) - \sum_j k_{ij} \cdot \rho_i(t_{k-1}) \right) \cdot \Delta t + \rho_i(t_{k-1}) \quad (26)$$

where k means the k th nanosecond from the pulse start. The Monte Carlo simulations were performed using laser pulses containing only the noise of a specific frequency band. As shown in Fig. 4, the noise suppression capability for different frequency bands is reflected by the root-mean-square error (RMSE) for the signal. Because the simulated laser power RMSE is set to 1, the RMSE of signal equals to the transfer coefficient μ . According to the maximum power of the laser in the actual experiment, the simulation condition we designed is that the pumping rate is 70 MHz, and the optimal integration time is 300 ns. From Fig. 4, we arrived at the following conclusions: for the overall characteristics of the DD methods, the noise suppression ability of the DD method is mainly in the range below 10^4 Hz and greater than 10^6 Hz. For the noise of these two different frequency bands, the principle of suppression is different. The low-frequency noise can be considered as a dc amount relative to the pulse sequence that can be eliminated by differential methods. High-frequency band, noise suppression is achieved due to the average effect of integration. However, for noise with a frequency close to the pulse frequency, this differential method fails to suppress it.

According to the theoretical analysis, we know that Methods-1a and -1b cannot completely eliminate the effect of light fluctuation on spin readout. The theoretical results can also be reflected in the simulation. For frequencies below

10^2 Hz, it can be seen from Fig. 4 that the noise suppression of Methods-1a and 1b is worse than that of Method-2. Unlike the theoretical analysis, Method-1 is superior to Method-2 in the range of 10^2 – 10^5 Hz. This phenomenon can be explained as follows: compared with Methods-1a and 1b, the additional reference pulse S^1 brings additional optical noise. Hence, the effect of Method-2 is worse than Method-1a. The disadvantage of Method-2 is that there is a frequency band of 0– 10^4 Hz. However, within 10^2 Hz, the effect of this drawback is lower than the effect of insufficient suppression of the optical power of Methods-1a and 1b, so it is only reflected at 10^2 – 10^4 Hz. Overall, Methods-1a and 1b are less affected by high-frequency noise, while Method 2 is better for low-frequency noise suppression.

IV. MODIFIED METHOD

Because both methods have intrinsic limitations, we propose a modified method to overcome them. According to (25), reducing $\mu = 0$ to the minimum is needed for making the SNR reach the photon shot noise limit. The specific idea of the modified model is to compensate for the lower ability of Method-1a in suppressing the optical power fluctuations by finding the first-order component of μ using the Taylor expansion. The theoretical SNR of the modified method obtained in this way can be close to the photon shot noise limit, because $\mu^2 \text{Var}(\Gamma) \rightarrow 0$.

The reasons for not selecting Method-2 for processing are as follows: 1) the disadvantage of introducing the extra noise compared with Method-1a cannot be eliminated; 2) the noise accompanying the microwave pulse further reduces the SNR due to the introduction of the second microwave pulse; and 3) Method-2 increases the time of a single sequence due to the introduction of additional pulses, resulting in a further setback in sensitivity. The expression of Method-1a can be modified as follows:

$$\frac{S - S^1}{S^1} = \frac{(P - P^1)}{g(\Gamma) + P^1}. \quad (27)$$

Because the change in pumping rate is small, we can use the Taylor expansion for analysis

$$\frac{S - S^1}{S^1}(\Gamma_0 + \Delta\Gamma) = \frac{S - S^1}{S^1} - g'(\Gamma_0) \left(\frac{S - S^1}{S^1} \right)^2 \Delta\Gamma. \quad (28)$$

From (28), we get the first-order item of μ , that is, $g'(\Gamma_0) \left(\frac{S - S^1}{S^1} \right)^2$. The change in the steady-state population C is used to represent the change in the light intensity $\Delta\Gamma$. The relationship between the light intensity fluctuation $\Delta\Gamma$ and the steady-state population fluctuation ΔC can be obtained by setting a modified factor ε

$$\varepsilon = \frac{\Delta\Gamma}{\Delta C} g'(\Gamma_0). \quad (29)$$

As the excited state population C is proportional to fluorescence. ΔC is represented by the fluctuation of steady-state fluorescence power which is experimentally measured at the end of the repumping pulse. The final modified relationship

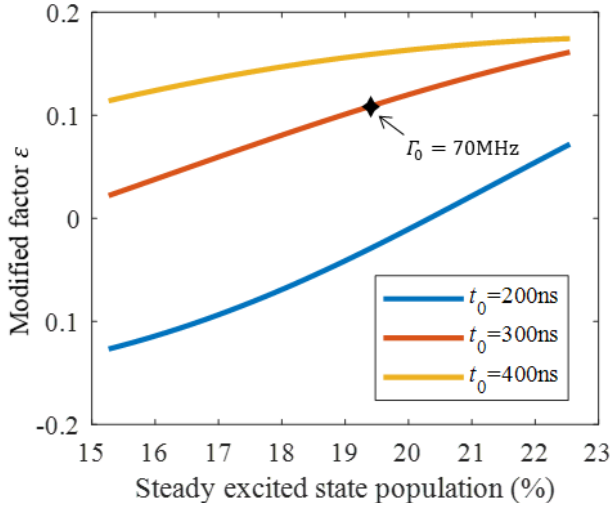


Fig. 5. Variation in modified factor ε with steady excited state under different integration times. ε corresponding to the simulation condition is marked as black star.

can be expressed as

$$\text{Signal} = \frac{S - S^1}{S^1} - \left(\frac{S - S^1}{S^1} \right)^2 \varepsilon \Delta C. \quad (30)$$

From (29), to solve ε , we need to solve $\Delta\Gamma/\Delta C$ and $g'(\Gamma_0)$. The expression of C is obtained by solving $A = 0$, as in (31), shown at the bottom of the next page.

Because $\Delta\Gamma$ is small, the following linear relationship can be considered to be satisfactory:

$$\frac{\Delta\Gamma}{\Delta C} = \frac{d\Gamma}{dC}. \quad (32)$$

According to (11), $g'(\Gamma) = (d(w_2^i/(w_1^i - w_2^i))/d\Gamma)$, which can be solved from the derivation of (7) as follows:

$$dW = d[U_1 \cdots U_5]^{-1} = -Wd[U_1 \cdots U_5]^{-1}W \quad (33)$$

and the derivation of U is

$$\frac{dU_i}{dA_{kl}} = \sum_{j \neq i} \frac{(U_i)_k (U_j)_l}{E_i - E_j} U_j. \quad (34)$$

There Γ -related matrix elements are A_{11} , A_{22} , A_{31} , and A_{42} . Using (33) and (34), $g'(\Gamma)$ can be solved by simple derivative rules. Different integration time t_0 selection causes the coefficient ε to change differently. According to the above calculation, 300 ns is the optimal integration time at the simulation condition $\Gamma_0 = 70$ MHz. Hence, the value of $\varepsilon = 0.111$ corresponding to 300 ns is used, as shown in Fig. 5.

In this way, the noise suppression capability can be approximately 2.1 times better than method-2 in the full measurement frequency bandwidth (0–10⁴ Hz) and approximately 27 times better than method-1a low frequency (1 Hz), as shown in Fig. 6.

Sensitivity is an important evaluation indicator for quantum sensing based on NV center, and thus we also analyzed the sensitivity of the modified method. Because this modified method does not require additional measurement time compared with the conventional methods but improves the SNR,

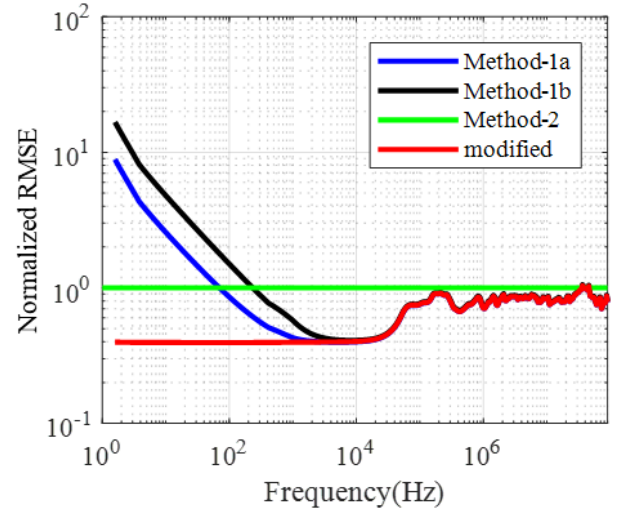


Fig. 6. Simulation comparison of the noise suppression capability of different frequency bands by different DD methods. The red curve represents the modified method and is lower than all other methods, especially in the range of 0–100 Hz.

this method will certainly improve sensitivity. A semi-physical simulation of magnetic sensing sensitivities of the photon shot noise theoretical limit, method-1a and the modified method is conducted. The simulation is to use the Ramsey sequence for dc magnetic field measurement. The simulation conditions are as follows: dephasing time $T_2^* = 500$ ns, single measurement time 10 μ s, and fluorescence 10⁹ counts/ms, which are consistent with the experimental condition in this article. Combined with the measured laser noise characteristics and the noise suppression capability obtained by the above analysis and sensitivity analysis in [27], the sensitivities are obtained for different methods, as shown in Fig. 7. The simulation results are consistent with our analysis. For shot noise limit, the minimum detectable magnetic field declines with \sqrt{t} , which leads to a shot-noise-limited sensitivity of 0.29 nT/Hz^{1/2}. For actual sensitivity, as the integration time increases, the sensitivity of Method-1a deteriorates significantly due to the increase in optical power noise and can only reach 1.25 nT/Hz^{1/2} under the measurement time of 1 s. The correction method can significantly reduce the effect of optical noise, so that the sensitivity reaches about 0.49 nT/Hz^{1/2}, which is corresponding to a 2.56-fold improvement in sensitivity.

V. EXPERIMENTAL TEST

To verify the practical effect of this method, we carried out experimental verification. The experimental setup is shown in Fig. 8. The pumping light was produced by a 532(±1)-nm laser (CNI MSL-FN-532-100 mW) with a maximum power of 100 mW and long-term stability rms <2%. The power spectral density of the laser noise is shown in Fig. 9. The laser power is adjusted by a combination of $\lambda/2$ wave plate mounted on a motorized precision rotation mount (Thorlabs PRM1/MZ8) and polarization beam splitter (PBS). The laser pulses are controlled by AOM (Gooch & Housego 3200-1911) which is driven by Gooch & Housego AODR 1200AF-DIFO-1.0 with the center frequency at 200 MHz. The objective lens is 60 \times /0.8 NA and with 0.17-mm working distance.

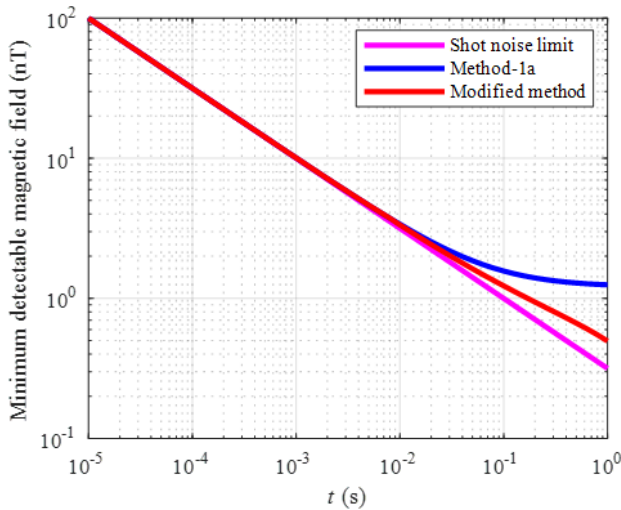


Fig. 7. Semi-physical simulation results of sensitivity.

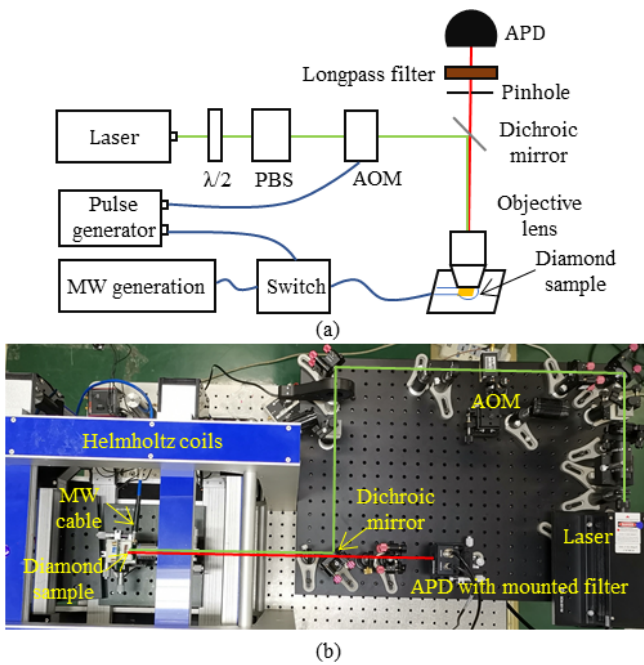


Fig. 8. (a) Schematic of experimental apparatus. The green line represents the excitation light path and the red line represents fluorescence. (b) Photograph of the experimental setup. The key components are labeled in the graph.

An avalanche photodiode (Thorlabs APD120A2/M) is used for fluorescence detection. The fluorescence data are recorded by a high-speed transient recorder (Spectrum M4i.4450-x8) with 500-MHz sampling rate, which is fast enough for accurate pulse signal measurement. A static magnetic field is produced by in-house developed Helmholtz coils which can generate a magnetic field of up to 50 Gauss in an arbitrary direction. The microwave source is a synthesized signal generator (Mini-Circuits SSG-6000RC), the frequency resolution of which is

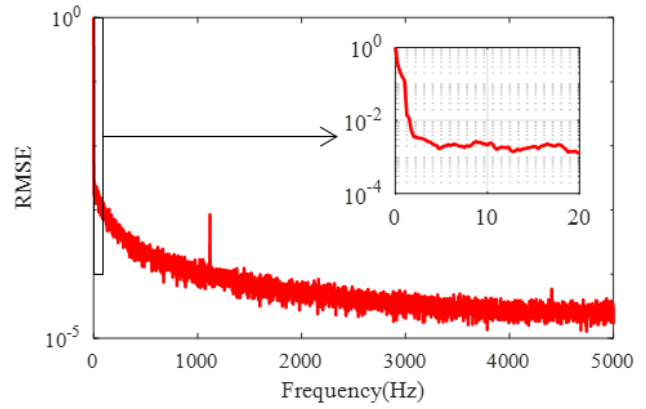


Fig. 9. Spectrum analysis of laser noise; the illustration is the result of low frequency.

less than 6 Hz, and the microwave is amplified by a microwave amplifier (ZHL-16W-43_S+), the maximum output power of which is 16 W. The microwave pulse is controlled by a microwave switch (zasw-2-50DR+). The microwave pulse is fed to the diamond through a home-made microwave antenna. All pulses are generated by a pulse generator (SpinCore PBESR-PRO-500) with 2-ns time resolution which is accurate enough in this article. The diamond sample is a high-pressure high-temperature (HPHT) type-Ib diamond (Element Six) under 5×10^{17} ea/cm² with 10-MeV electron irradiation and 2-h annealing at 800°. The initial substitutional nitrogen concentration in the diamond is labeled less than 200 ppm [36].

The modified method was experimentally verified using two approaches. The first approach performed the same normalized noise spectrum analysis as the simulation. Unlike the simulation results in Fig. 5, the experimental results also include photon shot noise. Through experiments, it is seen that the magnitude of the microwave noise is less than the optical power noise. Hence, optical noise is the main contributor, which is consistent with the application conditions of our modified method. As shown in Fig. 10(a), the original signal is very noisy at low frequencies due to optical power noise and detection noise ($1/f$ noise). With the modified method, the low-frequency noise is further suppressed. In this way, the transfer coefficient μ is reduced by about 38% (dc 10 Hz). This improvement is lower than in the simulation result. This is because the $1/f$ noise of the detection in the low-frequency band also affects the performance of the system. However, the detection noise does not satisfy the laser noise response law we analyzed earlier. The reason is that it is not a change in the fluorescence of the optical noise passing through the NV system, but the noise of the detector itself, which can be easily eliminated by directly using Method-1a, and our simulation does not consider the detection noise.

$$C(\Gamma) = \frac{(k_{35}k_{52} + k_{45}k_{51})\Gamma}{kk_{35}k_{52} + kk_{45}k_{51} + k_{35}k_{45}(k_{52} + k_{51}) + (k_{35}k_{52} + k_{45}k_{51} + k_{35}k_{45})\Gamma}. \quad (31)$$

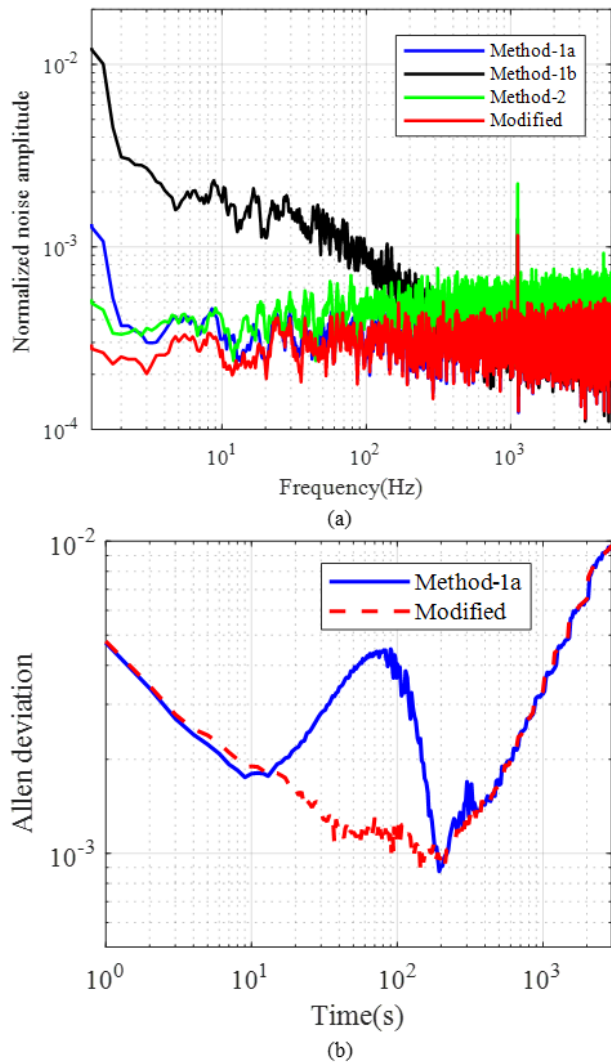


Fig. 10. (a) Noise spectrum analysis of the experimental results of different methods. (b) Blue solid curve and red dashed curve represent the Allen variance results of Method-1a and modified method, respectively.

The second verification method used the Allen variance to analyze the laser power drift suppression capability at very low frequencies. The laser power drift is due to the imperfection of the control circuit and the environmental fluctuation such as temperature drift. In this experiment, this drift is with a period on the order of 100 s and is the main factor of RMSE, and thus it mainly worsens the long-term performance. The modified method also achieves a correction for low-frequency drift compared with Method-1a and improves the SNR by 43.4% compared with Method-1a, as shown in Fig. 10(b). The rise at the end of the Allen variance is caused by the slow drift of the experiment apparatus, such as gradual deviations of optic mounts. Thus, it cannot be reduced by any DD method.

VI. CONCLUSION

This article uses the rate equations to analyze the optical dynamics of the NV center and find its analytical solution. With the proposed solution, a complete mathematical analysis of the existing spin pulse DD method is performed and a linear relationship between fluorescence and spin

polarization is obtained. Furthermore, the shortcomings of the two conventional DD spin readout methods in different frequency bandwidths are discussed. Based on these observations, an improved differential method is proposed, with the advantages of high-frequency noise suppression of the DD method with two laser pulses and low-frequency noise suppression of the DD method with three laser pulses. The modified method increases the noise suppression capability by a factor of 2.1 in theory. The spin readout experiment shows that the final SNR was improved by approximately 43.4%. Through the Allen analysis of variance, we achieved considerable complete suppression of periodic fluctuations in optical power compared with conventional methods. Our modified method does not depend on the specific experimental equipment or specific type of excitation sources, such as laser and led, and thus it can be widely applied to various pulsed NV center ensemble spin applications. The theoretical analysis of the spin readout method in NV center through optical rate equation solution approach is also instructive and meaningful to continuous-wave spin readout methods. Moreover, this spin readout method can be ported to other optical-driven spin systems expediently, such as spin readout of silicon carbide [37].

ACKNOWLEDGMENT

The authors would like to thank Prof. W. Dai for beneficial discussions.

REFERENCES

- [1] J. Zhao *et al.*, "Determination of spin polarization in spin-exchange relaxation-free atomic magnetometer using transient response," *IEEE Trans. Instrum. Meas.*, to be published.
- [2] X. Zhang, J. Qin, Y. Wang, and C. Chen, "A fast identification on the spin-exchange relaxation-free regime of atomic magnetometer exploiting measurement on gyromagnetic ratio," *IEEE Trans. Instrum. Meas.*, vol. 68, no. 4, pp. 1157–1164, Apr. 2019.
- [3] S. Schmitt *et al.*, "Submillihertz magnetic spectroscopy performed with a nanoscale quantum sensor," *Science*, vol. 356, no. 6340, pp. 832–837, May 2017.
- [4] T. Wolf *et al.*, "Subpicotesla diamond magnetometry," *Phys. Rev. X*, vol. 5, no. 4, Oct. 2015, Art. no. 041001.
- [5] I. V. Fedotov *et al.*, "Fiber-based thermometry using optically detected magnetic resonance," *Appl. Phys. Lett.*, vol. 105, no. 26, Dec. 2014, Art. no. 261109.
- [6] J. Wang *et al.*, "High-sensitivity temperature sensing using an implanted single nitrogen-vacancy center array in diamond," *Phys. Rev. B, Condens. Matter*, vol. 91, no. 15, Apr. 2015, Art. no. 155404.
- [7] H. J. Mamin *et al.*, "Nanoscale nuclear magnetic resonance with a nitrogen-vacancy spin sensor," *Science*, vol. 339, no. 6119, pp. 557–560, Feb. 2013.
- [8] T. Staudacher *et al.*, "Nuclear magnetic resonance spectroscopy on a (5-nanometer)³ sample volume," *Science*, vol. 339, no. 6119, pp. 561–563, Feb. 2013.
- [9] J. F. Barry *et al.*, "Optical magnetic detection of single-neuron action potentials using quantum defects in diamond," *Proc. Nat. Acad. Sci. USA*, vol. 113, no. 49, pp. 14133–14138, Dec. 2016.
- [10] A. Gruber, A. Dräbenstedt, C. Tietz, L. Fleury, J. Wrachtrup, and C. V. Borczyskowski, "Scanning confocal optical microscopy and magnetic resonance on single defect centers," *Science*, vol. 276, no. 5321, pp. 2012–2014, Jun. 1997.
- [11] A. D. Hopper, J. H. Shulevitz, and C. L. Bassett, "Spin readout techniques of the nitrogen-vacancy center in diamond," *Micromachines*, vol. 9, no. 9, p. 437, Aug. 2018.
- [12] L. Xu *et al.*, "High-efficiency fluorescence collection for NV-center ensembles in diamond," *Opt. Express*, vol. 27, no. 8, pp. 10787–10797, Apr. 2019.

- [13] N. H. Wan *et al.*, "Efficient extraction of light from a nitrogen-vacancy center in a diamond parabolic reflector," *Nano. Lett.*, vol. 18, no. 5, pp. 2787–2793, Mar. 2018.
- [14] K. Sasaki *et al.*, "Broadband, large-area microwave antenna for optically detected magnetic resonance of nitrogen-vacancy centers in diamond," *Rev. Sci. Instrum.*, vol. 87, no. 5, May 2016, Art. no. 053904.
- [15] N. Zhang *et al.*, "Microwave field uniformity impact on DC magnetic sensing with nv ensembles in diamond," *IEEE Sensors J.*, vol. 19, no. 2, pp. 451–456, Jan. 15, 2019.
- [16] L. Robledo, L. Childress, H. Bernien, B. Hensen, P. F. Alkemade, and R. Hanson, "High-fidelity projective read-out of a solid-state spin quantum register," *Nature*, vol. 477, no. 7366, pp. 574–578, Sep. 2011.
- [17] F. M. Hrubesch, G. Braunbeck, M. Stutzmann, F. Reinhard, and M. S. Brandt, "Efficient electrical spin readout of NV⁻ centers in diamond," *Phys. Rev. Lett.*, vol. 118, no. 3, Jan. 2017, Art. no. 037601.
- [18] Y. Dumeige *et al.*, "Magnetometry with nitrogen-vacancy ensembles in diamond based on infrared absorption in a doubly resonant optical cavity," *Phys. Rev. B, Condens. Matter*, vol. 87, no. 15, Apr. 2013, Art. no. 155202.
- [19] B. D'Anjou, and W. A. Coish, "Optimal post-processing for a generic single-shot qubit readout," *Phys. Rev. A, Gen. Phys.*, vol. 89, no. 1, Jan. 2014, Art. no. 012313.
- [20] A. Gupta, L. Hacquebard, and L. Childress, "Efficient signal processing for time-resolved fluorescence detection of nitrogen-vacancy spins in diamond," *J. Opt. Soc. Amer. B, Opt. Phys.*, vol. 33, no. 3, pp. B28–B34, 2016.
- [21] M. Steiner, P. Neumann, J. Beck, F. Jelezko, and J. Wrachtrup, "Universal enhancement of the optical readout fidelity of single electron spins at nitrogen-vacancy centers in diamond," *Phys. Rev. B, Condens. Matter*, vol. 81, no. 3, Jan. 2010, Art. no. 035205.
- [22] G. Waldherr *et al.*, "High-dynamic-range magnetometry with a single nuclear spin in diamond," *Nature Nanotech.*, vol. 7, no. 2, pp. 105–108, Feb. 2012.
- [23] B. D'Anjou, L. Kuret, L. Childress, and W. A. Coish, "Maximal adaptive-decision speedups in quantum-state readout," *Phys. Rev. X*, vol. 6, no. 1, Feb. 2016, Art. no. 011017.
- [24] E. Magesan, J. M. Gambetta, A. D. Córcoles, and J. M. Chow, "Machine learning for discriminating quantum measurement trajectories and improving readout," *Phys. Rev. Lett.*, vol. 114, no. 20, May 2015, Art. no. 200501.
- [25] L. Rondin, J.-P. Tetienne, T. Hingant, J.-F. Roch, P. Maletinsky, and V. Jacques, "Magnetometry with nitrogen-vacancy defects in diamond," *Rep. Prog. Phys.*, vol. 77, no. 5, May 2014, Art. no. 056503.
- [26] C. Zhang *et al.*, "Vector magnetometer based on synchronous manipulation of nitrogen-vacancy centers in all crystal directions," *J. Phys. D, Appl. Phys.*, vol. 51, no. 15, Apr. 2018, Art. no. 155102.
- [27] J. R. Maze *et al.*, "Nanoscale magnetic sensing with an individual electronic spin in diamond," *Nature*, vol. 455, no. 7213, pp. 644–647, Oct. 2008.
- [28] K. Ambal and R. D. McMichael, "A differential rate meter for real-time peak tracking in optically detected magnetic resonance at low photon count rates," *Rev. Sci. Instrum.*, vol. 90, no. 2, Feb. 2019, Art. no. 023907.
- [29] J. R. Maze *et al.*, "Properties of nitrogen-vacancy centers in diamond: The group theoretic approach," *New J. Phys.*, vol. 13, no. 2, Feb. 2011, Art. no. 025025.
- [30] M. W. Doherty, N. B. Manson, P. Delaney, and L. C. L. Hollenberg, "The negatively charged nitrogen-vacancy centre in diamond: The electronic solution," *New J. Phys.*, vol. 13, no. 2, Feb. 2011, Art. no. 025019.
- [31] G. Thiering and A. Gali, "Theory of the optical spin-polarization loop of the nitrogen-vacancy center in diamond," *Phys. Rev. B, Condens. Matter*, vol. 98, no. 8, Aug. 2018, Art. no. 085207.
- [32] M. L. Goldman *et al.*, "Phonon-induced population dynamics and inter-system crossing in nitrogen-vacancy centers," *Phys. Rev. Lett.*, vol. 114, no. 14, Apr. 2015, Art. no. 145502.
- [33] L. Robledo, H. Bernien, T. Van der Sar, and R. Hanson, "Spin dynamics in the optical cycle of single nitrogen-vacancy centres in diamond," *New J. Phys.*, vol. 13, no. 2, Feb. 2011, Art. no. 025013.
- [34] H. A. R. El-Ella, S. Ahmadi, A. M. Wojciechowski, A. Huck, and U. L. Andersen, "Optimised frequency modulation for continuous-wave optical magnetic resonance sensing using nitrogen-vacancy ensembles," *Opt. Express*, vol. 25, no. 13, pp. 14809–14821, 2017.
- [35] J. P. Tetienne *et al.*, "Magnetic-field-dependent photodynamics of single NV defects in diamond: An application to qualitative all-optical magnetic imaging," *New J. Phys.*, vol. 14, no. 10, Oct. 2012, Art. no. 103033.
- [36] C. Zhang *et al.*, "Dependence of high density nitrogen-vacancy center ensemble coherence on electron irradiation doses and annealing time," *J. Phys. D, Appl. Phys.*, vol. 50, no. 50, Dec. 2017, Art. no. 505104.
- [37] W. F. Koehl, B. B. Buckley, F. J. Heremans, G. Calusine, and D. D. Awschalom, "Room temperature coherent control of defect spin qubits in silicon carbide," *Nature*, vol. 479, pp. 84–87, Nov. 2011.
- [38] T. Häberle, D. Schmid-Lorch, F. Reinhard, and J. Wrachtrup, "Nanoscale nuclear magnetic imaging with chemical contrast," *Nature Nanotech.*, vol. 10, no. 2, pp. 125–128, Jan. 2015.

Jixing Zhang received the B.E. degree in instruments science and technology from Beihang University, Beijing, China, in 2015, where he is currently pursuing the Ph.D. degree.

His current research interests include the quantum sensing based on nitrogen-vacancy center in diamond.

Heng Yuan is currently an Associate Professor with the Research Institute of Frontier Science, Beihang University, Beijing, China, and the Key Laboratory of Ministry of Industry and Information Technology on Quantum Sensing Technology, Beijing.

His current research interests include quantum precision measurement and micro/nano device.

Ning Zhang received the Ph.D. degree from the School of Instrumentation and Optoelectronics Engineering, Beihang University, Beijing, China.

She is currently an Assistant Research Fellow with the Zhejiang Lab, Hangzhou, China. Her current research interests include solid-state spin materials, microwave sensors, atom magnetometer, and quantum precision measurement.

Lixia Xu received the bachelor's degree from the College of Instrumentation and Electrical Engineering, Jilin University, Jilin, China, in 2014. She is currently pursuing the Ph.D. degree with the School of Instrumentation Science and Optoelectronics Engineering, Beihang University, Beijing, China.

Her current research interests include quantum sensors.

Guodong Bian received the B.Sc. degree from Shandong University, Jinan, China, in 2016. He is currently pursuing the Ph.D. degree with the School of Instrumentation Science and Opto-electronics Engineering, Beihang University, Beijing, China.

His current research interests include the quantum sensing and quantum information processing based on the nitrogen-vacancy in diamond and other promising defect complexes in solid states.

Pengcheng Fan received the B.Sc. degree in applied physics from the Department of Physics, Beijing Institute of Technology (BIT), Beijing, China, in 2015. He is currently pursuing the Ph.D. degree from the School of Instrumentation Science and Optoelectronics Engineering, Beihang University, Beijing.

His current research interests include diamond color center quantum manipulation and quantum sensing.

Mingxin Li received the bachelor's degree from the School of Automation, Northwestern Polytechnical University, Shanxi, China, in 2017. He is currently pursuing the Ph.D. degree with the School of Instrumentation Science and Optoelectronics Engineering, Beihang University, Beijing, China.

His current research interests include quantum sensors and quantum information.

Zhi Zhan is currently pursuing the bachelor's degree with the School of Instrument and Optoelectronic Engineering, Beihang University, Beijing, China.

His current research interests include circuit design.

Kan Yu is currently a lecturer in Internet of Things with the Department of Computer Science and Information Technology, La Trobe University, Melbourne, VIC, Australia. His current research interests include industrial Internet-of-Things, and reliable and low-latency industrial wireless communications and real-time industrial communications.